Single-lap shear bond tests on Steel Reinforced Geopolymeric Matrix-concrete joints

Francesco Bencardino[a], Antonio Condello[a,*], Ashraf F. Ashour[b]

[a]*Department of Civil Engineering, University of Calabria, Via P. Bucci, Cubo 39B, Rende 87036, Italy*

[b]*School of Engineering, University of Bradford, Richmond Road, Bradford BD7 1DP, United Kingdom*

Abstract

Nowadays Fiber Reinforced Polymers (FRPs) represent a well-established technique for rehabilitation of Reinforced Concrete (RC) and masonry structures. However, the severe degradation of mechanical properties of FRP under high temperature and fire as well as poor sustainability represents major weak points of organic-based systems. The use of eco-friendly inorganic geopolymeric matrices, alternative to the polymeric resins, would be highly desirable to overcome these issues. The present work aims to investigate the bond characteristic of a novel Steel Reinforced Geopolymeric Matrix (SRGM) strengthening system externally bonded to a concrete substrate having low mechanical properties. SRGM composite material consists of stainless steel cords embedded into a fireproof geopolymeric matrix. Single-lap shear tests by varying the bonded length were carried out. The main failure mode observed of SRGM-concrete joints was debonding at the fiber-matrix interface. Test results also suggest the effective bond length. On the basis of the experimental results, a cohesive bond-slip law was proposed.

Keywords: A. Fabrics/textiles; B. Debonding; B. Fibre/matrix bond; C. Analytical modelling.

1. Introduction

Fiber Reinforced Polymers (FRPs) materials are the most common type of composite systems used for structural strengthening and rehabilitation applications of Reinforced Concrete (RC) structures. FRPs are comprised of continuous fibers (usually carbon, glass, or aramid) and an organic resin, typically epoxy, as a matrix. The researchers [1-3] and civil engineers [4, 5] are well-acquainted with the use of FRP composites Externally Bonded (EB) to RC members, and are eager to explore innovative materials that

[*]Corresponding author. Tel.: +39 0984496948. E-mail address: antonio.condello@unical.it

could lead to more sustainable alternatives to traditional composites without compromising the advantages of such retrofitting systems. Promising newly developed types of matrices, that are potentially represent a more sustainable, and durable alternative than epoxy, are the so-called inorganic matrix [6-9]. They can be used both with traditional [6] or innovative reinforcing strips/sheets [10-12]. Among these, novel steel strengthening strips, made of stainless or Ultra High Tensile Strength Steel (UHTSS) cords [13, 14], poliparafenilenbenzobisoxazolo [15, 16] and basalt fabrics [17] are now available in the construction industry. Different inorganic-based strengthening systems for RC structures were proposed, for example Textile Reinforced Concrete (TRC) [18, 19], Textile Reinforced Mortar (TRM) [20], Fiber Reinforced Cementitious Matrix (FRCM) [11, 21], Fiber Reinforced Grout (FRG) [22-24]. Some studies highlighted both the effectiveness of inorganic based composite materials as EB strengthening system and the different bond behavior and load transfer mechanisms compared to FRP system [16, 25, 26, 27]. As regards to FRCM systems, friction between fiber filaments and between fibers and matrix was observed after the debonding process initiates [28, 29]. Furthermore, a specific qualification method was proposed by Ascione et al. [30].

Within the broad category of inorganic matrices, geopolymers have raised some interest in recent years [31]. They are inorganic aluminosilicates produced by alkali activation solutions and source materials. Thus, geopolymers are manufactured using activated industrial waste materials such as fly ash in the presence of sodium hydroxide and sodium silicate solutions. The geopolymeric matrices have significant advantages compared to the traditional epoxy resin used for FRP system, such as: excellent resistance to corrosion, high value of transition temperature, no emission of toxic gases under intense fire, excellent durability even in strong aggressive conditions (coastal areas, deicing salts, acid rain) and high resistance against sulfates [8, 9, 24, 32]. A further advantage of the geopolymeric matrices compared to epoxy adhesives is related to their inorganic silico-aluminate nature, which makes these materials similar and alternative to cementitious materials, due to high mechanical properties and environmental advantages. In fact, the cement industry contributes around 6% of all CO_2 that is responsible for about 65% of global warming emissions [32], causing significant environmental issues. As a result, it is necessary to find new inorganic materials alternative to cementitious mortars which are environmentally stressful. To this end, geopolymers are a breakthrough development providing an essential alternative to cementitious materials, using novel environmentally friendly materials.

The use of geopolymer concrete in new RC members [33, 34] and geopolymeric matrices in the repair and strengthening of existing structures [24, 32] has been already investigated. With reference to the rehabilitation, two main applications were addressed: the use of geopolymeric mortars as repairing layer [32] or as binding agent to insure the adhesion between the external reinforcing sheets/strips/laminates and concrete substrate [24, 32]. When the geopolymeric matrix is used to embedded steel strips, the strengthening composite system is labeled as Steel Reinforced Geopolymeric Matrix (SRGM) [35, 36]. The studies available in literature show that geopolymer-based systems can be successfully used in strengthening applications of RC members [7, 9, 24, 35, 36], although their behavior is different from FRP composites due to differences in the debonding failure mechanism. Debonding failures are critical in strengthening applications because they can be brittles, and can control the overall performance of the system by triggering global member failure. With FRP composites, it is well-known that debonding typically occurs at the adhesive-concrete interface and usually involves a thin layer of the concrete substrate. Research available on debonding of steel reinforcing strips embedded into inorganic matrices is very limited. In general, the debonding was observed at matrix-steel cords interface [9, 24, 35, 36]. Consequently, the substrate, on which the composite is applied, could not play a key role in the design of the strengthening system. A complete understanding of the mechanism of interfacial load transfer of SRGM system bonded to concrete substrate is critical to design and has not yet been analyzed.

This paper presents the results of an experimental investigation aimed to study the interfacial behavior and stress-transfer mechanism of the SRGM composite EB to a concrete substrate. To this end, single-lap shear bond tests were carried out. In order to simulate substrates of existing old RC structures, the specimens were cast with low concrete strength. This research is needed for the development and/or validation of analytical models to calculate the effective bond length, which can be used to evaluate the load carrying capacity of the interface.

2. Experimental program

The experimental campaign was carried out at the “Laboratory of Materials and Structural testing” of the University of Calabria (Italy). It is a part of a wider in-progress experimental program aimed at investigating the bond behavior of SRGM-concrete joints as well as the structural performance of full scale RC beams strengthened with this innovative system [35, 36]. In this paper, the results of twelve

single-lap shear tests, with variable bonded lengths, are presented and analyzed. Detailed information about the geometry and mechanical properties of the test specimens, the strengthening system and the test set-up are given in the following sections.

2.1. Geometric and mechanical properties

The single-lap shear test specimens comprised of the composite SRGM system bonded to a concrete prism as shown in fig. 1. The concrete prisms were 150 mm wide x 200 mm deep x 600 mm long. The composite SRGM system was bonded to a 150 mm x 600 mm concrete face. The specimens were labeled with the bonded length (l_b) followed by "S" (if present), which indicates that the specimen was equipped with strain gages.

The concrete compressive cylinder strength (f_{cm}) was evaluated by testing six cylindrical samples (150 mm x 300 mm) at 28 days and the average value was 16.8 MPa. Splitting tensile tests were also carried out at 28 days on six cylindrical samples (150 mm x 300 mm) and the average tensile strength (f_{ctm}) was 1.7 MPa.

2.2. SRGM Strengthening system

The SRGM composite material consists of a stainless steel strip (Fig. 2(a)) embedded in an inorganic fireproof matrix (Fig. 2(b)). The properties of the steel strip provided by the manufacturer and/or trading company [37] are given in Table 1. It is a unidirectional reinforcing fabric made of stainless cords, particularly resistant to corrosion, suitable for interventions on substrates subject to rising damp and/or exposure to aggressive environments. The base material used for the manufacturing of steel fabrics is the same as the one used for tires. Therefore, a design process of the steel fabrics using the disposed worn tires will be environmentally friendly as well as the manufacturing process of geopolymeric matrices [38]. The properties of the matrix are given in the technical data sheet [39] and are summarized in Table 2. It is a polymers-based inorganic mineral with the addition of synthetic fibers, ready to use with the addition of 1 liter of water per 5 kg (Fig. 2(b)), and suitable for structural repairs of deteriorated cover concrete being able to be applied with thicknesses between 2 and 40 mm.

The main advantages of the polymer-based inorganic matrix are: high mechanical strength for both short and long curing, strong adhesion to concrete substrate, high resistance against sulfates, excellent

durability even in sever aggressive conditions (coastal areas, deicing salts, acid rain), excellent resistance to corrosion and high value of transition temperature (about 800°C).

The use of geopolymeric matrices in external strengthening applications is not yet widely known and used in practical applications, as it could potentially be, due to some critical issues that characterize these applications. Manufacturing of geopolymers represents the main issue [6]. So far, good mechanical and physical properties of geopolymeric composites were obtained by controlling the curing conditions at high temperature and pressure. The present work investigates the SRGM-concrete interface behavior on specimens cured at room temperature and atmospheric pressure.

2.3. Surface preparation and bond procedure

Before bonding of the external SRGM reinforcing system, faces of concrete blocks were carefully cleaned in order to remove dust, loose particles, oil stains, and other parts that could affect bonding. Subsequently, the concrete surface was subjected to moist sandblasting and hydraulic scouring. The matrix was only applied to the bonded area of the embedded fibers and to bond the composite to the concrete substrate. The matrix was applied from the edge of the external longitudinal cords on one side of the strip to the edge of external longitudinal cords on the other side of the strip. A 3-4 mm layer of matrix (internal layer) was applied using molds to control the composite width and thickness (Fig. 3(a)). A single layer of steel strip was applied onto the matrix, and the cords were pressed onto the matrix to assure proper impregnation (Fig. 3(b)). A second 3-4 mm external layer of matrix was applied over the steel strip (Fig. 3(c)). The bonded width was constant for all specimens (b_f = 50 mm), whereas the bonded length (l_b) of the composite was varied from 100 mm to 400 mm.

2.4. Test set-up and instrumentation

The single-lap shear test set-up, which is commonly used to study the bond characteristics of FRP/FRCM-concrete joints [15, 28, 29, 40] was adopted in this study. The classical push-pull configuration was used, in which the SRGM composite was pulled out of a restrained concrete prism (Fig. 4(a)). The concrete prism was restrained against movement by a steel plate bolted to the testing machine base. A steel plate was inserted to distribute the pressure to the prism. Tests were conducted under displacement control (0.0033 mm/s according to [30]) using a servo-hydraulic universal testing

machine. Assuming that the strain of concrete prism is neglected, the global slip may be defined as the relative displacement between points on the strip just outside the composite bonded area and the adjacent surface of the concrete prism (Fig. 4(b)). Global slip was measured using two linear variable displacement transducers (LVDTs). The LVDTs reacted off of a thin aluminum L-shaped plate that was attached to the steel cords adjacent to the beginning of the bonded area as shown in Fig. 4(c). The average of the two LVDT measurements was used to calculate the global slip. Furthermore, aluminum plates were attached to the end of the reinforcing strip with an epoxy resin to grip the steel cords during the tests. In order to measure the material strains of the steel strip, strain gages were attached along the bonded length. To apply the strain gages to the steel cords, slots were created during the application of the external layer of matrix in the locations of the strain gages (Fig. 4(c)). To avoid damage to the strain gages, the latter were installed after the hardening of the matrix. All the data obtained from load cell, strain gages, and LVDTs were automatically recorded through a data acquisition system with a frequency of 2 Hz.

3. Experimental results

3.1. Load-global slip response and failure modes

The load-global slip (*F*-*s*) curves for all tested specimens are shown in Fig. 5. It should be noted that the curves are quite similar and the ultimate global slip value depends on the bonded length. In fact, for largest bonded lengths, the highest slips were recorded. The values of the maximum load and the maximum strain recorded along the reinforcing strip, for all the tested specimens, are given in Table 3. The maximum values were recorded for the specimen 400S (F_{max} = 7.90 kN, ε_{max} = 6.65 ‰), respectively. Fig. 6 shows an idealized load-global slip response to that presented in Fig. 5 with the corresponding stages of the stress-transfer mechanism for bonded length greater than the effective bonded length (l_{eff}). The first part of the idealized *F*-*s* response is represented by a linear branch (OA) associated with elastic behavior of the interface (local bond-slip law, τ-*s*). After point A (Fig. 6), the response tends to be nonlinear; the interface between the fibers and the matrix exhibits some micro-damage, and the value of the applied load increases until the onset of debonding at the matrix–steel cords interface, which corresponds to point B (Fig. 6). After point B, a similar stress-transfer mechanism shifts along the bonded length, and the load remains approximately constant whereas the slip increases. As a result, the zone in which the stresses are transferred from the concrete substrate to the composite, labeled as stress transfer

zone (STZ), is fully established for bonded lengths greater than the effective bond length when the load reaches a value corresponding to debonding initiation. An increase of the global slip after initiation of the debonding process results in a simple translation of STZ further along the bonded length of the composite whereas its shape remains constant. It should be observed that the load-global slip response of the SRGM system bonded to concrete substrate is very similar to that of FRP-concrete joints [40].

However, the failure modes of SRGM-concrete joints are different compared with FRP-concrete joints. In fact, for FRP-concrete joints, it is well-known that interface crack propagation typically occurs within a thin layer of the substrate close to the FRP composite, and therefore the concrete mechanical and fracture properties and the surface treatment play an important role in the evaluation of the strengthening performance. However, for the SRGM-concrete joints, debonding was observed at steel cords-matrix interface and, only for the specimens 100 and 150S, debonding was developed at SRGM-concrete interface (Fig. 7). Consequently, the low mechanical properties of concrete substrate do not affect the bond performance of the strengthening system.

As suggested by Carloni et al. [28], different impregnation of the matrix along the steel cords and/or potential misalignment during the tests, could result in a non-uniform distribution of the applied load among the steel cords. The non-uniform load distribution was evaluated by calculating the rigid rotation of the L-shaped plate. By knowing the global slips in the left and right of the steel reinforcing strip at the loaded end (Fig. 8(a)), the rotation angle α can be calculated $\alpha = \arctan\frac{\Delta_L - \Delta_R}{70}$, where 70 mm is the distance between the two LVDTs (see Fig. 8(a)), Δ_L and Δ_R are the global slips recorded by LVDTs located at the left and right of the steel reinforcing strip, respectively. The load-α curves for all the tested specimens are calculated at each load stage and presented in Fig. 8(b). In general, the rotation angle ranges from -0.25° to 0.25° and, only for specimen 300S, the rotation angle is about 2°. This large rotation angle for specimen 300S indicates non-uniform distribution of the load and is deemed unacceptable. Therefore, the results for specimen 300S are not considered in the theoretical analysis presented below.

3.2. Effective bond length

The length needed to fully establish the STZ, i.e. the effective bond length (l_{eff}), can be defined as the distance between the two points of the nonlinear strain distribution in which the derivative of the strain

distribution function is zero close to the free end and constant close to the loaded end [27, 41]. Indeed, the zero value of derivative points out that load is not transferred and shear bond stress is equal to zero (stress-free zone). Instead, the constant value of derivative points out that debonding occurred and the shear bond stress is zero (fully-debonded zone). The average value of l_{eff} evaluated for the specimens equipped by strain gages is about 200 mm. For example, the strain distribution along the bonded length (l_{eff}) at different load levels, for the specimen 400S, is shown in Fig. 9. It should be noted that, at the maximum load (100% F_{max}), the strain recorded by the strain gage located at 50 mm is almost zero, whereas the strain recorded by the strain gage located at 250 mm is 6.65%. By using a nonlinear strain relationship fitting the actual strain distribution along the bonded length [41], it is easy to prove that the derivatives at 50 mm and at 250 mm are approximately zero and constant, respectively, concluding that the effective bond length is 200 mm.

Furthermore, being l_{eff} the length required to develop the maximum bond strength, the above result is also confirmed by analyzing the maximum load by varying the bonded length (Fig. 10). In fact, for bonded length higher than 200 mm, the maximum load is almost constant (specimens 200, 200S, 250, 250S, 300, 300S, 400, 400S), whereas for bonded length less than 200 mm the maximum load significantly lower (specimens 100, 100S, 150, 150S).

4. Analytical modeling for SRGM-concrete joint bond slip

It is well-known that the load carrying capacity of externally strengthened RC members is affected by premature failure caused by debonding of external reinforcing layer from concrete substrate. In order to evaluate the interfacial bond mechanisms and carry out accurate numerical simulations of SRGM strengthened RC members, an appropriate local bond-slip law (τ-s) is required as such model is not yet available in literature. In this study, a cohesive steel strip-matrix interface law is calibrated and validated against experimental data. The cohesive law defines the relationship between the shear stress at the interface and the relative movement between two points, one located in matrix and the other in stainless steel strip. The following assumptions were made in the analysis:

- SRGM strip is homogenous and linear elastic;
- the thickness and width of SRGM strip is constant along the bonded length;
- the interface is subjected only to shear loading and

- the strains in concrete and matrix are neglected.

Consequently, local slips can only occur at steel strip-matrix interface. This assumption is confirmed by experimental tests (Fig. 7).

As stated by Faella et al. [42], two approaches are available for calibration of an interface model based on experimental results: direct and indirect/inverse approaches. The procedure employed in this study is inspired to a direct approach.

Generally, in order to obtain the local bond-slip relationship from the direct single-lap shear bond test, many strain gages should be attached with a small interval (10 mm - 20 mm) on the surface of the reinforcing strip. As a result, the strain distribution along the interface corresponding to every step load can be obtained. Fig. 11 shows a sketch of test set-up required for single-lap shear bond tests. Assuming that the interval of strain gages (Δx) is a constant value (50 mm or 100 mm in this study), considering equilibrium, the bond stress can be obtained using the following expression:

$$\tau_i = E_f t_f \frac{d\varepsilon}{dx} = \frac{E_f t_f (\varepsilon_i - \varepsilon_{i-1})}{\Delta x} \tag{1}$$

where τ_i is the average interfacial bond stress in section i; ε_i and ε_{i-1} are the strain values of the i^{th} and $i\text{-}1^{th}$ gages arranged along the reinforcing strip, respectively, according to the reference system shown in Fig. 11; where E_f and t_f are the elastic modulus and thickness of the external reinforcement, respectively. The local slip between steel strip and matrix can be expressed as:

$$s_i = \frac{\Delta x}{2}\left(\varepsilon_0 + 2\sum_{j=1}^{i-1} \varepsilon_j + \varepsilon_i \right) \tag{2}$$

where s_i is the local slip between steel strip and matrix at section i; ε_0 is the strain in the steel strip at the free end of the bonded area (Fig. 11) and ε_j ($j=1, i$) is the strain value of the j^{th} strain gage arranged on the reinforcing strip. The free end slip strain can be assumed approximately as zero in the case of using a long bond length (greater than 200 mm in the present study).

An alternative method to obtain interfacial τ-s relationship without the necessity to record the strain distributions of SRGM system is used in the present study. It was proposed by Dai et al. [40] for FRP systems and assuming that at any location of an FRP-concrete interface, under the boundary condition of zero free end slip ($l_b \geq l_{eff}$), exists a unique τ-s relationship and a unique relationship between the strain of FRP sheets and interfacial slip. The latter can be expressed as follows:

$$\varepsilon = f(s) \tag{3}$$

where ε is the strain in FRP sheets at any location and s is the corresponding slip at that location. A first order differential calculus of ε to x yields the following equation:

$$\frac{d\varepsilon}{dx} = \frac{df(s)}{ds} f(s) \tag{4}$$

Therefore, using equation 4, the interfacial bond stress (equation 1) can be expressed as:

$$\tau = E_f t_f \frac{df(s)}{ds} f(s) \tag{5}$$

It should be noted that the bond-slip relationship can be determined if the relationship between strain and slip is defined. During the single-lap shear bond tests, the pullout forces and corresponding slips at the loaded end can be measured accurately through load cell and displacement transducers (LVDTs), respectively. As a result, the relationship between the strains of steel strip and the slips at the loaded end, namely as *f(s)*, can be directly obtained from the single-lap shear tests.

Assuming that the behavior of steel reinforcing strip is linear elastic up to brittle failure, the average value of strain at loaded end (Fig. 11) was calculated, at each load step, as:

$$\varepsilon = \frac{F}{E_f b_f t_f} \tag{6}$$

where F is the pullout force recorded by the load cell (see Fig. 11). The values of F are shown in Fig. 5. As stated in subsection 2.4, the slip s at loaded end was measured using two LVDTs. The experimental relationships between the strains of steel strips and interfacial slips at the loaded ends, for the specimens with bond length greater than the effective bond length (200 mm), are shown in Fig. 12. It was found that the exponential expression (equation 7), proposed by Dai et al. [40] for FRP system and based on an empirical assumption, fits very well the experimental results of the present study. Specifically, A and B are two parameters obtained through a nonlinear regression analysis.

$$\varepsilon = f(s) = A[1 - \exp(-Bs)] \tag{7}$$

By knowing the function *f(s)*, the bond stress-slip relationship (equation 5), the interfacial fracture energy (G_f) and the slip s_{max} corresponding to the maximum bond stress τ_{max} (at which $d\tau/ds=0$), can be obtained as follows:

$$\tau = A^2 B E_f t_f \exp(-Bs)[1 - \exp(-Bs)] \tag{8}$$

$$G_f = \int_0^{\infty} \tau ds = \frac{1}{2} A^2 E_f t_f \tag{9}$$

$$s_{\max} = 0.693 / B \tag{10}$$

By substituting equation 10 into equation 8, the maximum bond stress τ_{max} is equal to:

$$\tau_{\max} = 0.5 B G_f \tag{11}$$

For $l_b \geq l_{eff}$, the analytical maximum interfacial pullout force, $F_{max,AN}$ can be calculated by using the following relationship:

$$F_{\max,AN} = A E_f b_f t_f \tag{12}$$

The results and the analytical/experimental comparison in terms of debonding load are given in Table 4, for all test specimens.

Fig. 13 show the analytical/experimental comparison of the ε-s relationships. It should be noted that the analytical function (equation 7) fits very well the experimental response. The mean values of G_f, τ_{max} and s_{max}, calculated considering the specimens 200S, 200, 250S, 250, 300, 400S, 400 (Table 4), are equal to 0.54 N/mm, 1.76 MPa, and 0.12 mm, respectively. In general, the coefficient of determination R^2 is close to 1. This highlights that the regression curve fits quite well the experimental data. Furthermore, absolute average percentage error calculated on the debonding load is about 5.60%. In the previous calculations, the results obtained for specimen 300S were not considered due to excessive rotations during the test (Fig. 8), as explained earlier.

The cohesive bond-slip laws for all specimens listed in Table 4, excluding specimen 300S, together with the average law are shown in Fig. 14. Although the maximum interfacial strength (τ_{max}) of the cohesive laws is different for the tested specimens, the fracture energy is quite similar for all specimens (Table 4, Fig. 14). Furthermore, recent studies available in the literature [43] showed that the variation of the maximum interfacial strength (τ_{max}) do not have a strong influence on the numerical results.

The reliability of the bond-slip law was also checked through a theoretical prediction, by means of a fracture mechanics based model [44], of RC beams strengthened with SRGM system applied by innovative Inhibiting-Repairing-Strengthening (IRS) technique [35, 36]. For IRS-SRGM strengthened beams debonding at fiber-matrix interface, similar to the failure mode of the SRGM-concrete joints (Fig. 7), was observed during the experimental tests [35,36]. Therefore, the mean value of fracture energy (0.54 N/mm) was used in the theoretical model to calculate the energy dissipated due to debonding. It was

shown that the analytical results fit very well with the experimental ones [36], pointing out the reliability of the proposed bond-slip law. Further details regarding the fracture mechanics based model and theoretical/experimental comparisons are given in Gunes et al. [44] and Bencardino and Condello [36].

5. Conclusions

The bond behavior and shear transfer mechanisms of a new inorganic-based strengthening system bonded to concrete were experimentally and analytically investigated. Results obtained from single-lap shear bond tests, in terms of load-global slip response, debonding load, axial strains along reinforcing strip and failure modes, showed the effectiveness of the strengthening system. To simulate existing concrete substrate, the specimens were constructed with low concrete strength. On the basis of the obtained results, the following concluding remarks can be drawn:

- The load-global slip response of SRGM system bonded to concrete substrate is very similar to that of FRP-concrete joints.
- For SRGM-concrete joints, the debonding was observed at steel strip-matrix interface. As a result, the mechanical properties of concrete substrate do not affect the bond performance of the strengthening system. It is an interesting aspect of SRGM composite because the substrate on which the system is applied does not play a key role in the design of the strengthening system.
- The effective bond length for SRGM system is about 200 mm.
- A cohesive bond-slip law capable of simulating the interfacial behavior between steel cords/strip and inorganic matrix was calibrated and validated against the experimental results. The mean values of fracture energy, maximum shear bond stress and corresponding slip are equal to 0.54 N/mm, 1.76 MPa and 0.12 mm, respectively.

The study highlights the potentiality of the SRGM strengthening system. Nevertheless, further experimental and theoretical investigations are needed to consolidate the obtained results. Future work should investigate the bond and structural performances of SRGM systems under different environmental conditions, such as fire exposure and/or different temperature and pressure.

Acknowledgements

Part of the analyses were developed within the activities of Rete dei Laboratori Universitari di Ingegneria

Sismica (ReLUIS) for the research program funded by the Dipartimento di Protezione Civile (DPC), Progetto DPC/ReLUIS 2016 – AQ DPC/ReLUIS 2014-2016.

Special thanks are extended to Eng. Giuseppe Sposato for the assistance in the laboratory tests.

References

[1] Bakis CE, Bank LC, Brown VL, Cosenza E, Davalos JF, Lesko JJ, Machida A, Rizkalla SH, Triantafillou TC. Fiber reinforced polymer composites for construction - state-of-the-art review. Journal of Composites for Construction 2002; 6(2): 73-87.

[2] Bencardino F, Colotti V, Spadea G, Swamy RN. Holistic design of RC beams and slabs strengthened with externally bonded FRP laminates. Cement and Concrete Composites 2006; 28(10): 832-844.

[3] Ashour AF, El-Refaie SA, Garrity SW. Flexural strengthening of RC continuous beams using CFRP laminates. Cement and Concrete Composites 2004; 26(7): 765-775.

[4] ACI 440.2R-08. Guide for the Design and Construction of Externally Bonded FRP Systems for Strengthening Concrete Structures. American Concrete Institute, Farmington Hills, Michigan, USA, 2008.

[5] CNR-DT 200 R1/2013. Guide for the Design and Construction of Externally Bonded FRP Systems for Strengthening Existing Structures – Materials, RC and PC structures, masonry structures. Italian National Research Council, Rome, Italy, 2013.

[6] Giancaspro JW, Papakonstantinou CG, Balaguru P. Flexural response of inorganic hybrid composites with E-glass and carbon fibers. Journal of Engineering Materials and Technology 2010; 132: 1–8.

[7] Katakalos K, Papakonstantinou CG. Fatigue of Reinforced Concrete Beams Strengthened with Steel-Reinforced Inorganic Polymers. Journal of Composites for Construction 2009, 10.1061/(ASCE)1090-0268(2009)13:2(103).

[8] Kurtz S, Balaguru P. Comparison of inorganic and organic matrices for strengthening of RC beams with carbon sheets. Journal of Structural Engineering 2001; 127(1): 35–42.

[9] Papakonstantinou CG, Katakalos K. Flexural behavior of reinforced concrete beams strengthened with a hybrid inorganic matrix - steel fiber retrofit system. Structural Engineering and Mechanics

2009; 31(5): 1-19.

[10] Balsamo A, Nardone F, Iovinella I, Ceroni F, Pecce M. Flexural strengthening of concrete beams with EB-FRP, SRP and SRCM: Experimental investigation. Composites Part B: Engineering 2013; 46: 91-101.

[11] Babaeidarabad S, Loreto G, Nanni A. Flexural strengthening of RC beams with an externally bonded fabric-reinforced cementitious matrix. Journal of Composites for Construction 2014; 18(5): 04014009.

[12] Bencardino F, Condello A. Structural behaviour of RC beams externally strengthened in flexure with SRG and SRP systems. International Journal of Structural Engineering 2014; 5(4): 346-368.

[13] Barton B, Wobbe E, Dharani LR, Silva P, Birman V, Nanni A, Alkhrdaji T, Thomas J, Tunis G. Characterization of reinforced concrete beams strengthened by steel reinforced polymer and grout (SRP and SRG) composites. Materials Science & Engineering 2005; 412: 129-136.

[14] Bencardino F, Condello A. SRG/SRP-concrete bond-slip laws for externally strengthened RC beams. Composite Structures 2015; 132: 804-815.

[15] D'Antino T, Sneed LH, Carloni C, Pellegrino C. Influence of the substrate characteristics on the bond behavior of PBO FRCM-concrete joints. Construction and Building Materials 2015; 101: 838-850.

[16] D'Ambrisi A, Feo L, Focacci F. Bond-slip relations for PBO-FRCM materials externally bonded to concrete. Composites Part B: Engineering 2012; 43(8): 2938–2949.

[17] Campione,G, La Mendola L, Monaco A, Valenza A, Fiore V. Behavior in compression of concrete cylinders externally wrapped with basalt fibers. Composites Part B: Engineering 2015; 69: 576-586.

[18] Bruckner A, Ortlepp R, Curbach M. Textile reinforced concrete for strengthening in bending and shear. Materials and Structures 2006; 39: 741–748.

[19] Larbi AS, Agbossou A, Hamelin P. Experimental and numerical investigations about textile-reinforced concrete and hybrid solutions for repairing and/or strengthening reinforced concrete beams. Composite Structures 2013; 99: 152-162.

[20] Triantafillou TC, Papanicolau CG. Shear strengthening of reinforced concrete members with textile reinforced mortar (TRM) jackets. Materials and Structures 2006; 39: 85–93.

[21] Trapko T. Behaviour of fibre reinforced cementitious matrix strengthened concrete columns under

eccentric compression loading. Materials & Design 2014; 54: 947-954.

[22] Bencardino F, Condello A. Reliability and adaptability of the analytical models proposed for the FRP systems to the Steel Reinforced Polymer and Steel Reinforced Grout strengthening systems. Composites Part B: Engineering 2015; 76: 249-259.

[23] Napoli A, Realfonzo R. Reinforced concrete beams strengthened with SRP/SRG systems: Experimental investigation. Construction and Building Materials 2015; 93: 654-677.

[24] Menna C, Asprone D, Ferone C, Colangelo C, Balsamo A, Prota A, Cioffi R, Manfredi G. Use of geopolymers for composite external reinforcement of RC members. Composites Part B: Engineering 2013; 45: 1667–1676.

[25] Awani O, El Refai A, El-Maaddawy T. Bond characteristics of carbon fabric-reinforced cementitious matrix in double shear tests. Construction and Building Materials 2015; 101: 39-49.

[26] Donnini J, Corinaldesi V, Nanni A. Mechanical properties of FRCM using carbon fabrics with different coating treatments. Composites Part B: Engineering 2016; 88: 220-228.

[27] Ombres L. Analysis of the bond between Fabric Reinforced Cementitious Mortar (FRCM) strengthening systems and concrete. Composites Part B: Engineering 2015; 69: 418-426.

[28] Carloni C, D'Antino T, Sneed L, Pellegrino C. Role of the Matrix Layers in the Stress-Transfer Mechanism of FRCM Composites Bonded to a Concrete Substrate. Journal of Engineering Mechanics 2015; 141(6): 04014165.

[29] D'Antino T, Sneed LH, Carloni C, Pellegrino C. Effect of the inherent eccentricity in single-lap direct-shear tests of PBO FRCM-concrete joints. Composite Structures 2016; 142: 117-129.

[30] Ascione L, De Felice G, De Santis S. A qualification method for externally bonded Fibre Reinforced Cementitious Matrix (FRCM) strengthening systems. Composites Part B: Engineering 2015; 78: 497-506.

[31] Davidovits J. Geopolymer chemistry and applications. Institute Geopolymere, Morrisville; 2008.

[32] Vasconcelos E, Fernandes S, Barroso de Aguiar JL, Pacheco-Torgal S. Concrete retrofitting using metakaolin geopolymer mortars and CFRP. Construction and Building Materials 2011; 25: 3213–3221.

[33] Akbarnezhad A, Huan M, Mesgari S, Castel A. Recycling of geopolymer concrete. Construction and Building Materials 2015; 101: 152-158.

[34] Nguyen KT, Ahn N, Le TA, Lee K. Theoretical and experimental study on mechanical properties and flexural strength of fly ash-geopolymer concrete. Construction and Building Materials 2016; 106: 65-77.

[35] Bencardino F, Condello A. Innovative solution to retrofit RC members: Inhibiting-Repairing-Strengthening (IRS). Construction and Building Materials 2016; 117: 171-181.

[36] Bencardino F, Condello A. Eco-friendly external strengthening system for existing reinforced concrete beams. Composites Part B: Engineering 2016; 93: 163-173.

[37] ST2-0910. Range of stainless steel reinforcing fabrics for structural consolidation, Kimisteel INOX. Kimia S.p.A., 2015.

[38] Caggiano A, Xargay H, Folino P, Martinelli E. Experimental and numerical characterization of the bond behavior of steel fibers recovered from waste tires embedded in cementitious matrices. Cement and Concrete Composites 2015; 62: 146-155.

[39] ST1-0613. R4 Normal curing thixotropic geopolymeric mortar for rehabilitation in compliance with the marking requirements laid down by UNI EN 1504-3 for R4 mortars and the requirements for armor protection systems defined in EN 1504-7, Betonfix MONOLITE N. Kimia S.p.A., 2015.

[40] Dai J, Ueda T, Sato Y. Development of the nonlinear bond stress-slip model of fiber reinforced plastics sheet-concrete interfaces with a simple method. Journal of Composites for Construction 2005; 9(1): 52-62.

[41] Carloni C, Subramaniam KV. Application of fracture mechanics to debonding of FRP from RC members. American Concrete Institute 2012; 286(SP): 145-159.

[42] Faella C, Martinelli E, Nigro, E. Direct versus indirect method for identifying FRP-to-concrete interface relationships. Journal of Composites for Construction 2009; 13 (3): 226-233.

[43] Alfano G, Crisfield MA. Finite element interface models for the delamination analysis of laminated composites: mechanical and computational issues. International Journal for Numerical Methods in Engineering 2001; 50: 1701–1736.

[44] Gunes O, Buyukozturk O, Karaca E. A fracture-based model for FRP debonding in strengthened beams. Engineering Fracture mechanics 2009; 76: 1897-1909.

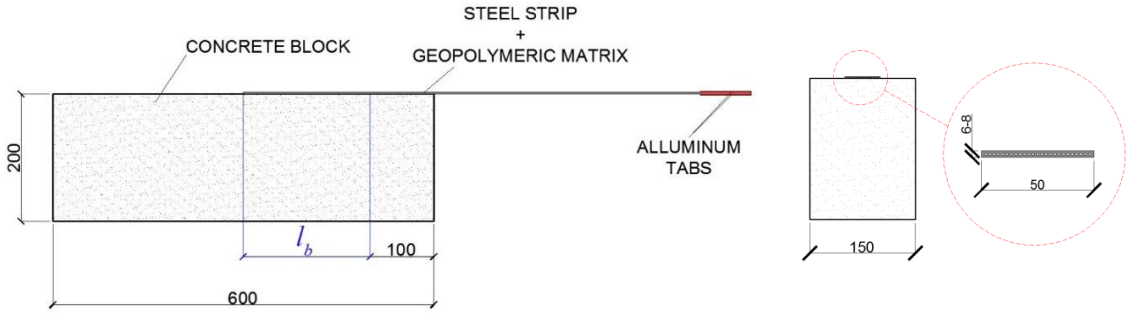

(a) (b)

Fig. 1. Geometrical details of test specimens: (a) Longitudinal section; (b) Transversal section (all dimensions are in mm).

(a) (b)

Fig. 2. SRGM composite system: (a) Unidirectional stainless steel strip; (b) Geopolymeric matrix.

(a) (b) (c)

Fig. 3. Bond procedure: (a) First internal layer of matrix; (b) Steel strip; (c) Second external layer of matrix.

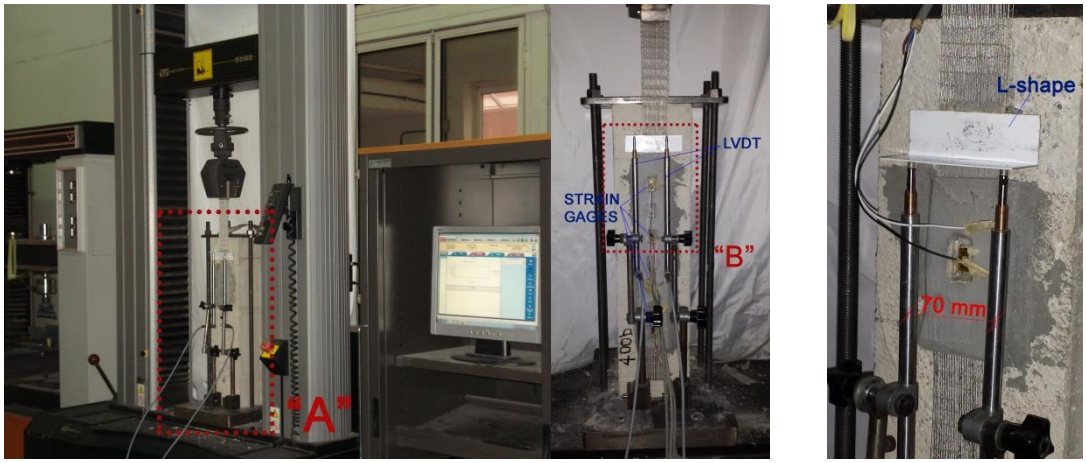

(a) (b) (c)

Fig. 4. Test set-up: (a) Testing machine; (b) Detail "A"; (c) Detail "B".

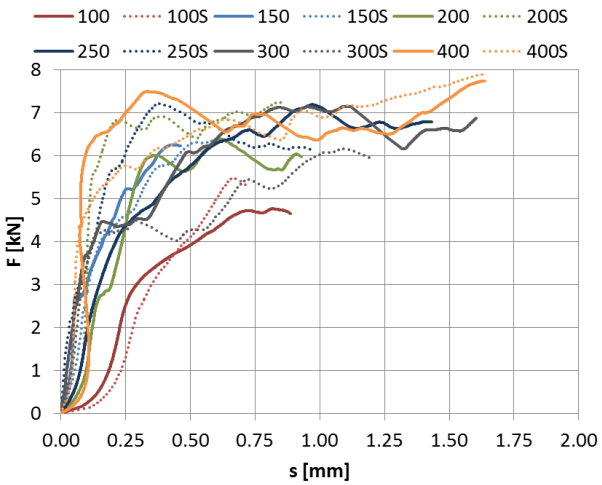

Fig. 5. Load-global slip curves.

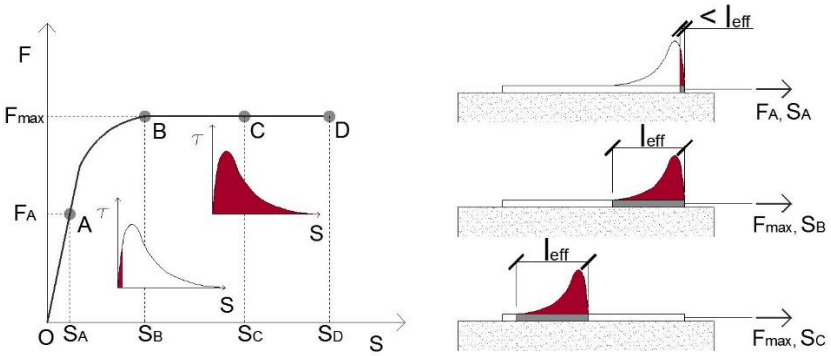

Fig. 6. Idealized load-global slip response.

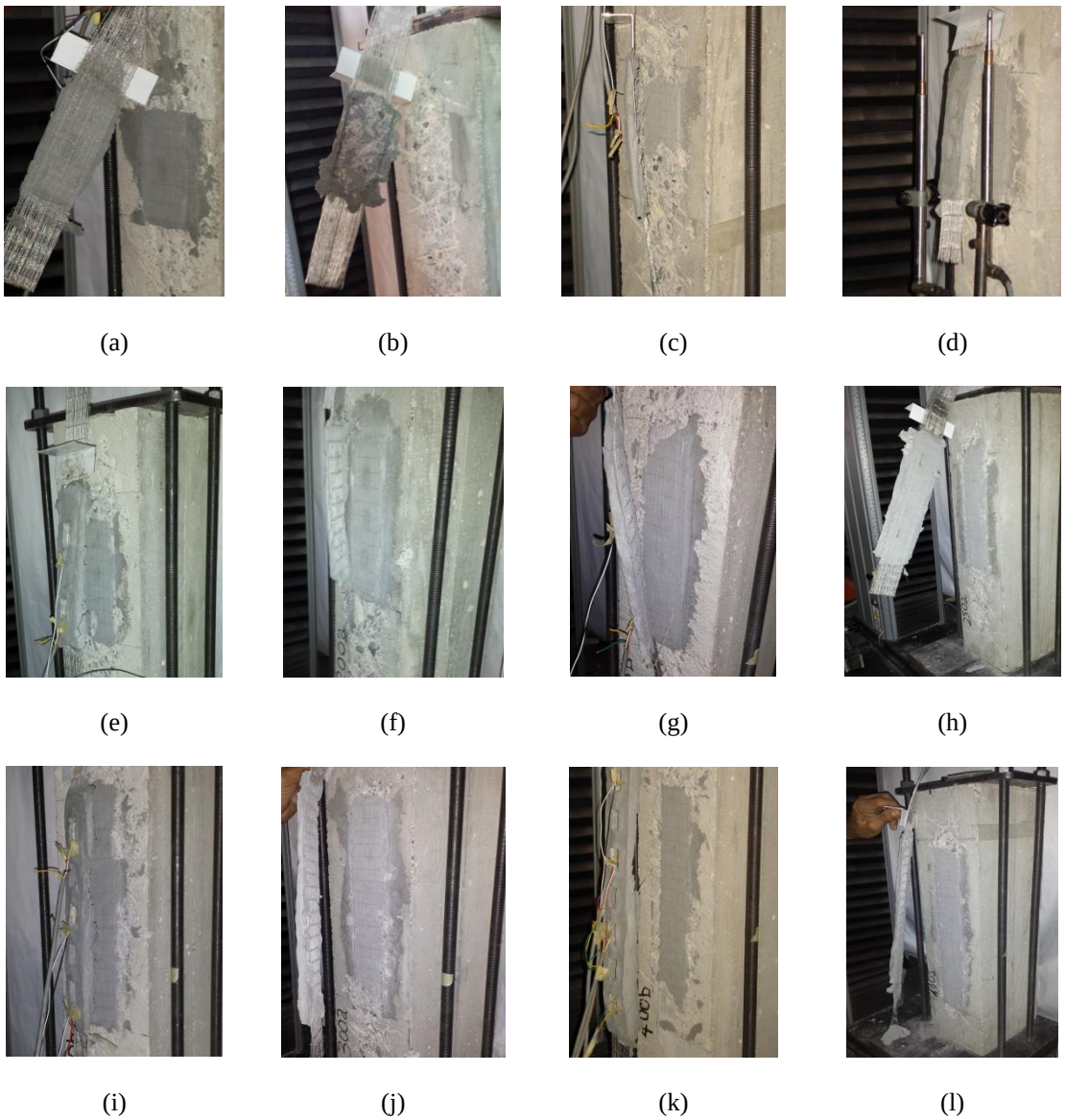

Fig. 7. Failure modes: (a) 100S; (b) 100; (c) 150S; (d) 150; (e) 200S; (f) 200; (g) 250S; (h) 250; (i) 300S; (j) 300; (k) 400S; (l) 400.

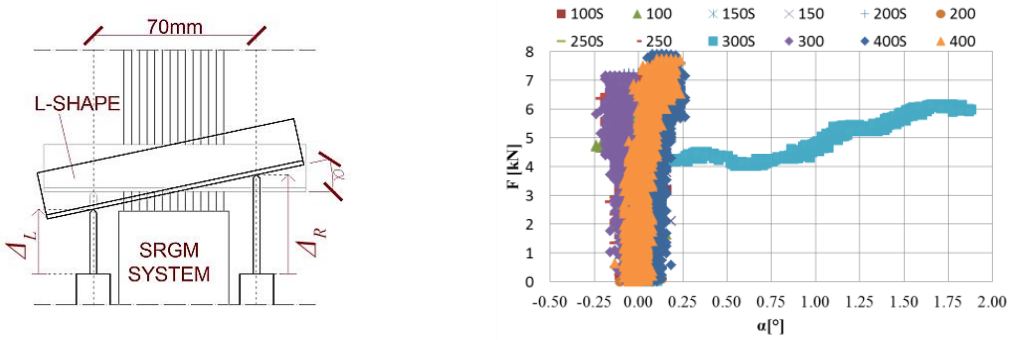

(a) (b)

Fig 8. Rotation angle of L-shaped plate: (a) LVDT position; (b) Load against rotation angle.

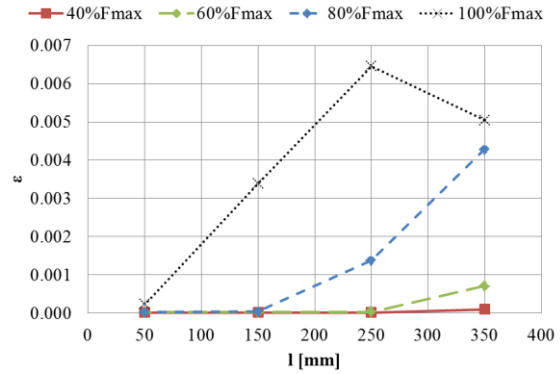

Fig. 9. Strain distribution along the bonded length (specimen 400S).

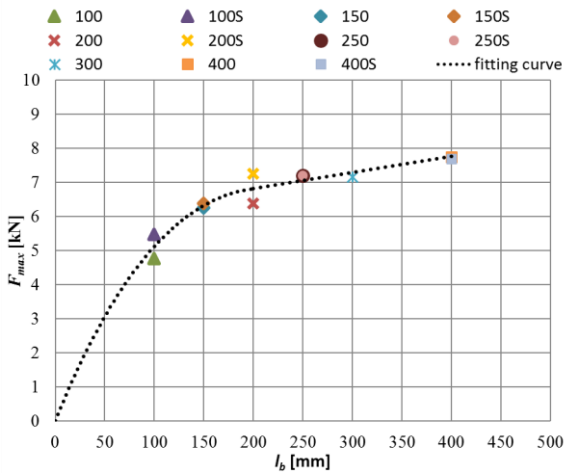

Fig. 10. Maximum load against the bonded length.

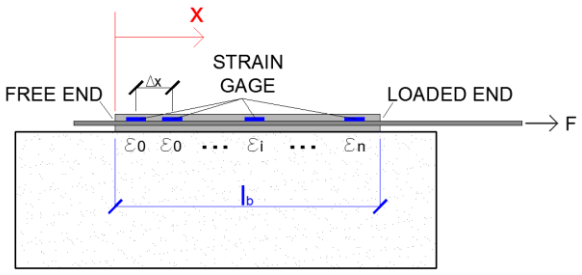

Fig. 11. Analytical modeling.

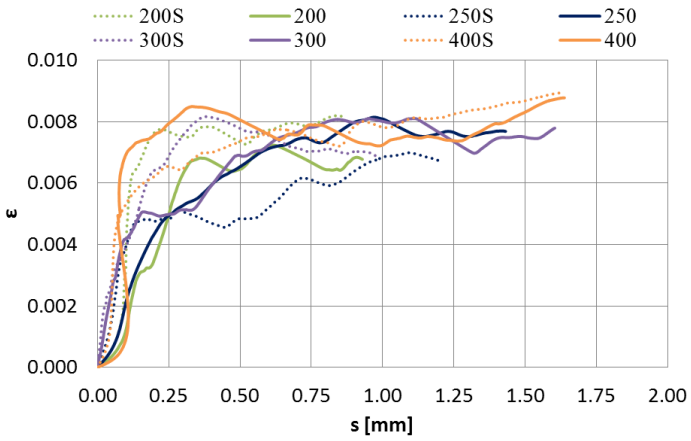

Fig. 12. Experimental strain-global slip curves at the loaded end.

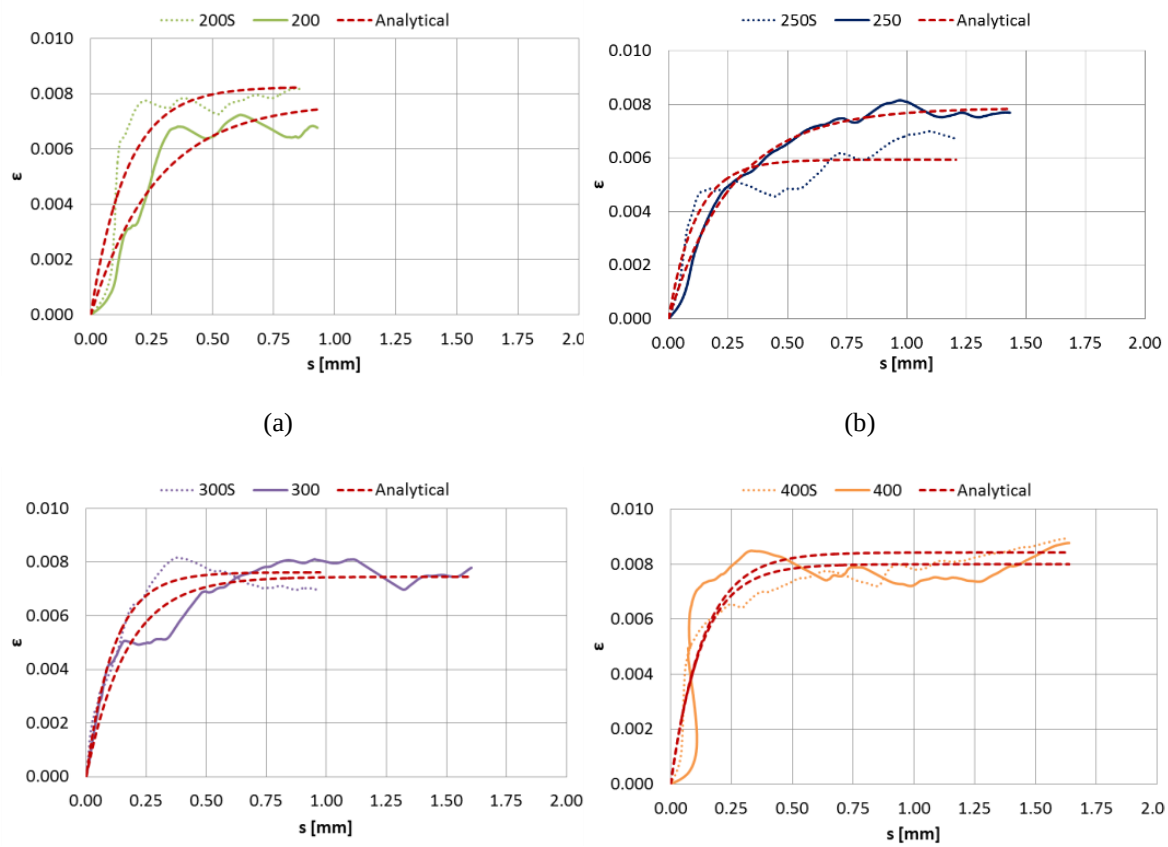

Fig. 13. Experimental/Analytical comparison of the fiber strain-global slip curves: (a) 200S/200; (b) 250S/250; (c) 300S/300; (d) 400S/400.

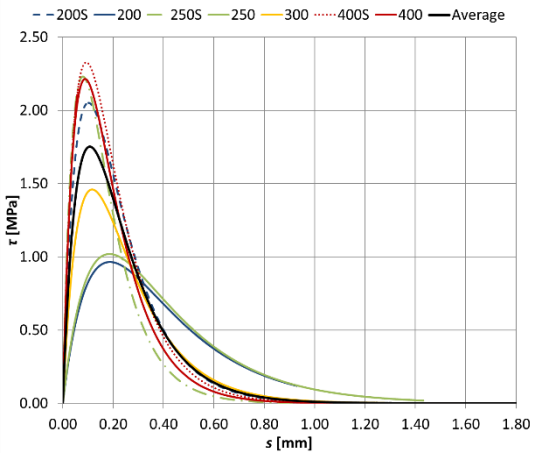

Fig. 14. Cohesive interface bond-slip law.

Table 1

Properties of unidirectional reinforcing stainless steel strips according to the manufacturer [37].

Property	Value
Grammage	2200 g/m^2
Fibre direction (warp – steel)	99 %
Fibre direction (weft)	1 %
Threads diameter	0.11 mm
Wire diameter	1.00 mm
Strip width	100 mm
Nominal thickness of the strip (t_f)	0.24 mm
Unitary resistance of the strip	380 N/mm
Resistance wires	1470 MPa
Modulus of elasticity wires (E_f)	73.5 GPa
Elongation at break wires	2.00 %

Table 2

Properties of inorganic matrix [39].

Property	Value
Compressive strength at 28 days	$\geq$ 45 MPa
Elastic secant modulus in compression	$\geq$ 20 GPa
Adhesion to concrete	$\geq$ 2 MPa
Granulometric interval	0.1 – 0.5 mm
Apparent volumetric mass of fresh mortar	2050 kg/m^3
Minimum application temperature	+5 °C

Table 3

Test results.

Specimen	Bond length, l_b [mm]	Maximum load, $F_{max,EXP}$ [kN]	Maximum strain, ε_{max} [‰]
100S	100	5.47	3.48
100		4.76	-
150S	150	6.38	4.58
150		6.25	-
200S	200	7.24	5.57
200		6.39	-
250S	250	7.20	6.24
250		7.19	-
300S	300	6.17	5.35
300		7.15	-
400S	400	7.90	6.65
400		7.74	-

Table 4

Analytical results and comparisons.

Specimen	A [‰]	B [mm^{-1}]	G_f [N/mm]	τ_{max} [N/mm^2]	s_{max} [mm]	R^2	$F_{max,\,EXP}$ [kN]	$F_{max,\,AN}$ [kN]	*Error* [%]
200S	8.31	6.82	0.60	2.05	0.10	0.91	7.24	7.28	0.55
200	7.60	3.70	0.52	0.96	0.18	0.90	6.39	6.78	6.04
250S	7.62	8.71	0.51	2.2	0.08	0.97	7.20	6.72	6.67
250	7.86	3.74	0.55	1.02	0.19	0.99	7.19	6.94	3.48
300S	5.93	8.69	0.31	1.35	0.08	0.91	6.17	5.23	15.24
300	7.50	5.95	0.49	1.46	0.12	0.88	7.15	6.57	8.11
400S	7.95	8.48	0.56	2.36	0.08	0.93	7.90	7.44	5.82
400	8.00	7.83	0.57	2.21	0.09	0.63	7.74	7.06	8.79

Figure captions

Fig. 1. Geometrical details of test specimens: (a) Longitudinal section; (b) Transversal section (all dimensions are in mm).

Fig. 2. SRGM composite system: (a) Unidirectional stainless steel strip; (b) Geopolymeric matrix.

Fig. 3. Bond procedure: (a) First internal layer of matrix; (b) Steel strip; (c) Second external layer of matrix.

Fig. 4. Test set-up: (a) Testing machine; (b) Detail "A"; (c) Detail "B".

Fig. 5. Load-global slip curves.

Fig. 6. Idealized load-global slip response.

Fig. 7. Failure modes: (a) 100S; (b) 100; (c) 150S; (d) 150; (e) 200S; (f) 200; (g) 250S; (h) 250; (i) 300S; (j) 300; (k) 400S; (l) 400.

Fig 8. Rotation angle of L-shaped plate: (a) LVDT position; (b) Load against rotation angle.

Fig. 9. Strain distribution along the bonded length (specimen 400S).

Fig. 10. Maximum load against the bonded length.

Fig. 11. Analytical modeling.

Fig. 12. Experimental strain-global slip curves at the loaded end.

Fig. 13. Experimental/Analytical comparison of the fiber strain-global slip curves: (a) 200S/200; (b) 250S/250; (c) 300S/300; (d) 400S/400.

Fig. 14. Cohesive interface bond-slip law.